CHEMISTRY OF MATERIALS
Article

Chem. Mater. **2010,** *22,* 3407–3417 3407
DOI:10.1021/cm100297q

Au Nanoparticles in Nanocrystalline TiO_2-NiO Films for SPR-Based, Selective H_2S Gas Sensing

Enrico Della Gaspera,[†] Massimo Guglielmi,[†] Stefano Agnoli,[‡] Gaetano Granozzi,[‡] Michael L. Post,[§] Valentina Bello,[‖] Giovanni Mattei,[‖] and Alessandro Martucci*[,†]

[†]*Dipartimento di Ingegneria Meccanica Settore Materiali, Università di Padova, Via Marzolo, 9, 35131 Padova, Italy,* [‡]*Dipartimento di Scienze Chimiche and INSTM Research Unit, Università di Padova, Via Marzolo, 1, 35131 Padova, Italy,* [§]*Institute for Chemical Process and Environmental Technology, National Research Council of Canada, 1200 Montreal Road, Ottawa, Ontario K1A 0R6, Canada, and* [‖]*Dipartimento di Fisica, Università di Padova, Via Marzolo, 8, 35131 Padova, Italy*

Received January 29, 2010. Revised Manuscript Received April 16, 2010

Thin films composed of Au nanoparticles dispersed inside a TiO_2-NiO mixed oxide matrix are prepared by the sol−gel method, resulting in nanostructured composites with a morphology and crystallinity that depend on synthesis parameters and thermal treatment. Their functional activity as hydrogen sulfide optical sensors is due to Au-localized surface plasmon resonance (SPR) which is reversible. The detection sensitivity is shown to be down to a few parts per million of H_2S, and almost no interference in response is observed during simultaneous exposure to CO or H_2, resulting in a highly sensitive and selective sensor for hydrogen sulfide detection. For mechanistic studies, experimental evidence using reaction product analysis and thin film surface characterization suggests a direct catalytic oxidation of H_2S over the $Au-TiO_2-NiO$ nanocomposite film.

Introduction

Hydrogen sulfide (H_2S) is a well-known toxic gas that can be produced or can be a byproduct of several processes such as oil refining, coal or natural gas manufacturing, fuel cells, or food processing industries. This gas is dangerous for human health even at low concentrations: exposure at 250 ppm can seriously injure the human body and even cause death,[1] so the threshold limit for human exposure is usually set by governmental legislation (for example, in the United States it is 10 ppm for every 10 min of exposure, with the exposure level decreasing with time).[2] In addition, H_2S can act as a poison that severely degrades the activity of catalysts and electrochemical devices.[3]

As a result, great effort has been spent in developing materials for highly sensitive and selective hydrogen sulfide sensors and in developing new efficient and low-cost devices capable of real-time fast detection of even very small amounts of H_2S; most of the literature in this field deals with resistive electrical sensor devices, where the active materials are powders[4−6] or thin[7,8] or thick films.[9,10] Most of the sensing materials reported in H_2S detection are CuO, SnO_2, ZnO, WO_3, or a combination of them.[11−26] Some others techniques are based on the

---

(1) Tao, W. H.; Tsai, C. H. *Sens. Actuators, B* **2002**, *81*, 237.
(2) Lawrence, N. S.; Davis, J.; Compton, R. G. *Talanta* **2000**, *52*, 771.
(3) Xiao, T.; An, L.; Zhang, W.; Sheng, S.; Xiong, G. *Catal. Lett.* **1992**, *12*, 287.
(4) Kapse, V. D.; Ghosh, S. A.; Chaudhari, G. N.; Raghuwanshi, F. C. *Talanta* **2008**, *76*, 610.
(5) Wang, Y.; Cao, J.; Kong, F.; Xia, H.; Zhang, J.; Zhu, B.; Wang, S.; Wu, S. *Sens. Actuators, B* **2008**, *131*, 183.
(6) Chaudhari, G. N.; Bambole, D. R.; Bodade, A. B.; Padole, P. R. *J. Mater. Sci.* **2006**, *41*, 4860.
(7) Rumyantseva, M.; Labeau, M.; Delabouglise, G.; Ryabova, L.; Kutsenoka, I.; Gaskov, A. *J. Mater. Chem.* **1997**, *7*(9), 1785.
(8) Ando, M.; Suto, S.; Suzuki, T.; Tsuchida, T.; Nakayarna, C.; Miurab, N.; Yamazoeb, N. *J. Mater. Chem.* **1994**, *4*, 631.
(9) Jain, G. H.; Patil, L. A.; Wagh, M. S.; Patil, D. R.; Patil, S. A.; Amalnerkar, D. P. *Sens. Actuators, B* **2006**, *117*, 159.
(10) Wang, Y.; Wang, S.; Zhao, Y.; Zhu, B.; Kong, F.; Wang, D.; Wu, S.; Huang, W.; Zhang, S. *Sens. Actuators, B* **2007**, *125*, 79.
(11) Sberveglieri, G.; Groppelli, S.; Nelli, P.; Perego, C.; Valdre, G.; Camanzi, A. *Sens. Actuators, B* **1998**, *55*, 86.
(12) Lin, H. M.; Hsu, C. M.; Yang, H. Y. *Sens. Actuators, B* **1994**, *22*, 63.
(13) Wagh, M. S.; Patil, L. A.; Seth, T.; Amalnerkar, D. P. *Mater. Chem. Phys.* **2004**, *84*, 228.
(14) Tamaki, J.; Maekawa, T.; Miura, N.; Yamazoe, N. *Sens. Actuators, B* **1992**, *9*, 197.
(15) Manorama, S.; Sarala Devi, G.; Rao, V. J. *Appl. Phys. Lett.* **1994**, *64*, 3163.
(16) Sarala Devi, G.; Manorama, S.; Rao, V. J. *J. Electrochem. Soc.* **1995**, *142*, 2754.
(17) Tamaki, J.; Shimanoe, K.; Yamada, Y.; Yamamoto, Y.; Miura, N.; Yamazoe, N. *Sens. Actuators, B* **1998**, *49*, 125.
(18) Vasiliev, R. B.; Rumyantseva, M. N.; Yakovlev, N. V.; Gaskov, A. M. *Sens. Actuators, B* **1998**, *50*, 186.
(19) Mangamma, G.; Jayaraman, V.; Gnanasekaran, T.; Periaswami, G. *Sens. Actuators, B* **1998**, *53*, 133.
(20) Yuanda, W.; Maosong, T.; Xiuli, H.; Yushu, Z.; Guorui, D. *Sens. Actuators, B* **2001**, *79*, 187.
(21) Wang, C.; Chu, X.; Wu, M. *Sens. Actuators, B* **2006**, *113*, 320.
(22) Berger, O.; Hoffmann, T.; Fischer, W. J. *J. Mater. Sci.* **2004**, *15*, 483.
(23) Maekawa, T.; Tamaki, J.; Miura, N.; Yamazoe, N. *J. Mater. Chem.* **1994**, *4*(8), 1259.
(24) Solis, J. L.; Saukko, S.; Kish, L. B.; Granqvist, C. G.; Lannto, V. *Sens. Actuators, B* **2001**, *77*, 316.
(25) Sarala Devi, G.; Manorama, S.; Rao, V. J. *Sens. Actuators, B* **1995**, *28*, 31.
(26) Niranjan, R. S.; Patil, K. R.; Sainkar, S. R.; Mulla, I. S. *Mater. Chem. Phys.* **2003**, *80*, 250.

detection of the products generated from the interaction of H_2S with the sensor materials, i.e., sulfide species analyzed by gas chromatography,[27−30] high-pressure liquid chromatography (HPLC),[31] or electrochemical methods.[32] An alternative innovative detection mode is related to optical gas sensing where the changes in the optical properties of the device are analyzed. Developing materials tailored to accomplish such a task is very relevant to current material science research. However, only few examples of optical H_2S sensors have been reported so far, and most of them depend on organic dyes or organic complexes of transition metals as active materials,[33−35] although some articles discussing fully inorganic optical gas sensors have been published.[36−38]

In this paper, we report the synthesis and characterization of TiO_2−NiO thin films containing Au nanoparticles (NPs) and the determination of their optical gas sensing properties toward different gases (H_2, CO, propane, and H_2S). While most of the literature concerning TiO_2−NiO nanocomposite materials deals with catalysis[39−42] and photocatalysis,[43−45] and other particular applications of these systems are electrochromism,[46−48] solar cells,[44,49] and supercapacitors,[50] only few gas sensing studies on similar material have been reported so far.[51−53] In particular, neither the optical gas sensing properties of TiO_2−NiO films nor studies on Au NPs dispersed inside TiO_2−NiO films have been reported. The two specific metal oxide components, i.e., TiO_2 and NiO, were selected for the nanocomposite thin films because of the known catalytic and sensing properties of these materials, and the embedding of Au NPs was performed to enhance the optical sensitivity of the nanocomposites. The results presented here indicate that the tested nanocomposite is particularly active and selective toward H_2S detection, and an explanation of the possible sensing mechanism is discussed.

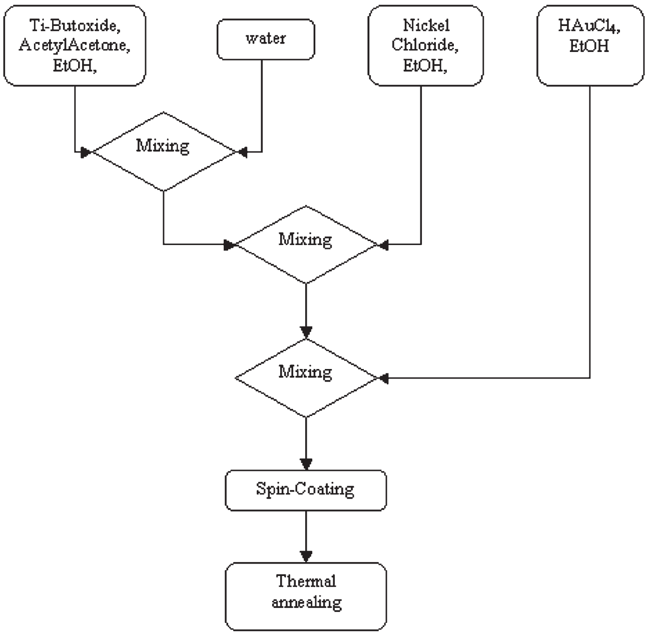

Figure 1. Scheme of the overall synthetic process developed to prepare TiO_2−NiO nanocomposite films.

Experimental Procedures

The nanocomposite films were obtained by the sol−gel method; different solutions were prepared according to the desired final composition of the sample. Figure 1 summarizes the overall synthetic procedure we adopted to obtain the final nanocomposite films. The precursor TiO_2 solution involved the controlled hydrolysis of titanium(IV) butoxide (TiBu) in a mixture of ethanol and water, in the presence of 2,4-pentanedione [or acetylacetone (AcAc)]. Acetylacetone coordinates the titanium precursor molecules through a slightly exothermic reaction, while ethanol decreases the overall viscosity of the solution. TiBu, AcAc, and ethanol were first mixed at 1:1.6:5 molar ratios and allowed to react with stirring for 20 min in a closed vessel, to create the AcAc−TiBu complex. Then water was added according to a 1:4 Ti:H_2O molar ratio, and the solution was left to stir for an additional 10 min. We prepared the precursor NiO solution separately by dissolving $NiCl_2 \cdot 6H_2O$ (nickel chloride hexahydrate) in ethanol and adding it to the TiO_2 solution with constant stirring, according to the desired Ti:Ni molar ratio (7:3, 5:5, or 3:7), and letting it stir for 20 min before deposition (hereafter called TiO_2−NiO solution). We prepared TiO_2−NiO films containing Au NPs by adding, 10 min before deposition, a solution of $HAuCl_4 \cdot 3H_2O$ (hydrogen tetrachloroaurate trihydrate) in ethanol to the TiO_2−NiO solution, leading to a 0.05 Au:(Ti + Ni) molar ratio. We prepared Au-free samples

---

(27) Ramstad, T.; Bates, A. H.; Yellig, T. J.; Borchert, S. J.; Mills, K. A. *Analyst* **1995**, *120*, 2775.
(28) Simo, R.; Grimalt, J. O. *J. Chromatogr., A* **1996**, *726*, 161.
(29) Radford-Knoery, J.; Cutter, G. A. *Anal. Chem.* **1993**, *65*, 976.
(30) Berube, P. R.; Parkinson, P. D.; Hall, E. R. *J. Chromatogr., A* **1999**, *830*, 485.
(31) Gru, C.; Sarradin, P. M.; Legoff, H.; Narcon, S.; Caprais, J. C.; Lallier, F. H. *Analyst* **1998**, *123*, 1289.
(32) Kroll, A. V.; Smorchkov, V. I.; Nazarenko, A. Y. *Sens. Actuators, B* **1994**, *21*, 97.
(33) Noor, U. M.; Uttamchandani, D. *J. Sol-Gel Sci. Technol.* **1998**, *11*, 177.
(34) Choi, M. M. F.; Hawkins, P. *Sens. Actuators, B* **2003**, *90*, 211.
(35) Wallace, K. J.; Cordero, S. R.; Tan, C. P.; Lynch, V. M.; Anslyn, E. V. *Sens. Actuators, B* **2007**, *120*, 362.
(36) Sarma, T. V. S.; Tao, S. *Sens. Actuators, B* **2007**, *127*, 471.
(37) Zhang, Z.; Jiang, H.; Xing, Z.; Zhang, X. *Sens. Actuators, B* **2004**, *102*, 155.
(38) Miao, Z.; Wu, Y.; Zhang, X.; Liu, Z.; Han, B.; Dinga, K.; An, G. *J. Mater. Chem.* **2007**, *17*, 1791.
(39) Rubinstein, A. M.; Dulov, A. A.; Slinkin, A. A.; Abramova, L. A.; Gershenzon, I. S.; Gorskaya, L. A.; Danyushevskii, V. J.; Dashevskii, M. I.; Klyachko-Gurvich, A. L.; Lavrovskaya, T. K.; Lafer, L. I.; Yakerson, V. I. *J. Catal.* **1974**, *35*(1), 80.
(40) Sohn, J. R.; Han, J. H. *Appl. Catal., A* **2006**, *298*, 168.
(41) Sohn, J. R.; Lee, S. G. *Catal. Lett.* **2008**, *120*, 116.
(42) Uchiyama, S.; Obayashi, Y.; Hayasaka, T.; Kawata, N. *Appl. Catal.* **1989**, *47*, 155.
(43) Sreethawong, T.; Suzuki, Y.; Yoshikawa, S. *Int. J. Hydrogen Energy* **2005**, *30*, 1053.
(44) Arakawa, H.; Sayama, K. *Res. Chem. Intermed.* **2000**, *26*(2), 145.
(45) Kamegawa, T.; Kim, T. H.; Morishima, J.; Matsuoka, M.; Anpo, M. *Catal. Lett.* **2009**, *129*, 7.
(46) Al-Kahlout, A.; Aegerter, M. A. *Sol. Energy Mater. Sol. Cells* **2007**, *91*, 213.
(47) Huang, H.; Lu, S. X.; Zhang, W. K.; Gan, Y. P.; Wang, C. T.; Yu, L.; Tao, X. Y. *J. Phys. Chem. Sol.* **2009**, *70*, 745.
(48) Martini, M.; Brito, G. E. S.; Fantini, M. C. A.; Craievich, A. F.; Gorenstein, A. *Electrochim. Acta* **2001**, *46*, 2275.
(49) Lee, Y. M.; Hsu, C. H.; Chen, H. W. *Appl. Surf. Sci.* **2009**, *255*, 4658.
(50) Xie, Y.; Huang, C.; Zhou, L.; Liu, Y.; Huang, H. *Compos. Sci. Technol.* **2009**, *69*, 2108.
(51) Arshak, K. I.; Cavanagh, L. M.; Gaidan, I.; Moore, E. G.; Clifford, S. A. *IEEE Sens. J.* **2007**, *7*(6), 925.
(52) Imawan, C.; Solzbacher, F.; Steffes, H.; Obermeier, E. *Sens. Actuators, B* **2000**, *68*, 184.
(53) Wisitsoraat, A.; Tuantranont, A.; Comini, E.; Sberveglieri, G.; Wlodarski, W. *Thin Solid Films* **2009**, *517*, 2775.

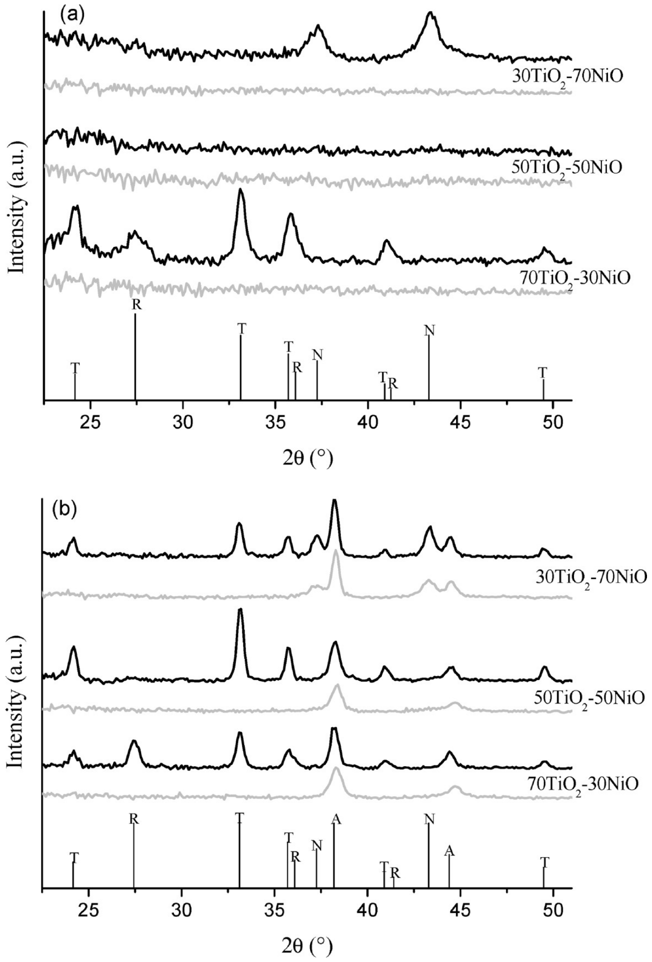

Figure 2. XRD pattern of (a) TiO_2−NiO and (b) Au−TiO_2−NiO nanocomposite films, annealed at 500 °C (gray line) and 600 °C (black line). Theoretical diffraction lines for TiO_2−rutile (R), NiO (N), $NiTiO_3$ (T), and Au (A) are shown at the bottom.

by diluting the TiO_2−NiO solution with ethanol to obtain the same precursor concentration of the Au-containing solution, kept constant at 50 g/L based on the nominal weight of TiO_2 and NiO. Pure TiO_2 and Au−TiO_2 samples were also prepared for the purpose of comparison, according to the same procedure, replacing the NiO solution with ethanol. In a typical synthesis for a 50:50 TiO_2−NiO sample, 0.55 mL of titanium butoxide was added to 0.47 mL of EtOH under stirring; 0.266 mL of AcAc was subsequently added and the solution stirred for 20 min, and then 0.117 mL of water was slowly added under vigorous stirring. In two separate vessels, 0.384 g of $NiCl_2 \cdot 6H_2O$ was dissolved in 2.95 mL of EtOH and 51 mg of $HAuCl_4 \cdot 3H_2O$ was dissolved in 0.647 mL of EtOH. The TiO_2 and NiO solutions were mixed under stirring, and the Au solution or 0.647 mL of EtOH was eventually added, leading to Au-containing or Au-free solutions, respectively. All the solutions were prepared in 10 mL glass vials.

The final solution was then deposited on either SiO_2 glass or Si substrates. The spin coating technique was chosen for film deposition, with the rotating speed ranging from 2500 to 4000 rpm at room temperature (20 °C) and under constant nitrogen flux to keep humidity under 5%, to prevent uncontrolled condensation of the TiO_2 matrix. Samples were annealed directly at 500 °C in air for 1 h in a preheated oven. When desired, subsequent treatment at 600 °C for 30 min was performed. In the following, we adopt the $X$$TiO_2$−(100−$X$)NiO classification to indicate the samples with different nominal compositions in X mole percent.

Table 1. Mean Crystallite Diameters Calculated According to the Scherrer Equation for the Diffraction Peaks of 70TiO_2−30NiO and 30TiO_2−70NiO Films Annealed at 600°C with and without Gold[a]

	diameter (nm)			
	70TiO_2−30NiO	70TiO_2−30NiO with Au	30TiO_2−70NiO	30TiO_2−70NiO with Au
TiO_2	10	15	−	−
$NiTiO_3$	12	17	−	−
NiO	−	−	6	15

[a] The 50TiO_2−50NiO film is not considered in this table because without gold it is still amorphous.

Samples were characterized with X-ray diffraction (XRD), scanning electron microscopy (SEM), transmission electron microscopy (TEM), X-ray photoemission spectroscopy (XPS), ultraviolet photoemission spectroscopy (UPS), spectroscopic ellipsometry, and UV−vis absorption. A detailed description of all the equipment and characterization techniques used and of the gas sensing apparatus is reported in the Supporting Information.

Results and Discussion

Chemical and Structural Characterization. Figure 2 shows X-ray diffraction (XRD) patterns for the different samples prepared in this study; TiO_2−NiO samples (Figure 2a) are completely amorphous at 500 °C, even after being annealed for 10 h (data not shown here), while crystalline phases are present at 600 °C. Similar sol−gel thin films obtained from different precursors show crystalline NiO peaks even at 400 °C, at variance with the results of our study.[54]

In detail, at 600 °C the Ti-rich sample 70TiO_2−30NiO shows both TiO_2−rutile (PDF 870920) and nickel titanate ($NiTiO_3$) peaks (PDF 760335), while the Ni-rich sample 30TiO_2−70NiO shows only NiO peaks (PDF 471049); a further annealing (for at least 2 h) at the same temperature leads also to the formation of the $NiTiO_3$ phase (data not shown here). The 50TiO_2−50NiO sample does not show any diffraction peak, even after being annealed at 600 °C, but as with the previous sample, an extended thermal treatment at 600 °C (2 h) leads to the formation of $NiTiO_3$ crystals (data not shown here).

All the samples containing Au (Figure 2b) show gold diffraction peaks (PDF 040714) at both 500 and 600 °C, indicating, as described in the literature, that reduction of gold ions inside a sol−gel oxide matrix during the annealing of the film (see below for details) occurs at quite low temperatures, usually below 200 °C.[55] It is also evident that the presence of Au NPs promotes the overall crystallization of the matrix: in fact, at 500 °C NiO nanocrystals are already present in the 30TiO_2−70NiO sample. This can be due to the very small lattice mismatch between the two cubic structures, which allows NiO to crystallize over gold nuclei (in a previous work,[56] we demonstrated the epitaxial growth of NiO over Au crystals inside a SiO_2

---

(54) Al-Kahlout, A.; Heusing, S.; Aegerter, M. A. *J. Sol-Gel Sci. Technol.* **2006**, *39*, 195.
(55) Sakka, S.; Kozuka, H. *J. Sol-Gel Sci. Technol.* **1998**, *13*, 701.
(56) Buso, D.; Guglielmi, M.; Martucci, A.; Mattei, G.; Mazzoldi, P.; Sada, C.; Post, M. *Cryst. Growth Des.* **2008**, *8*(2), 744.

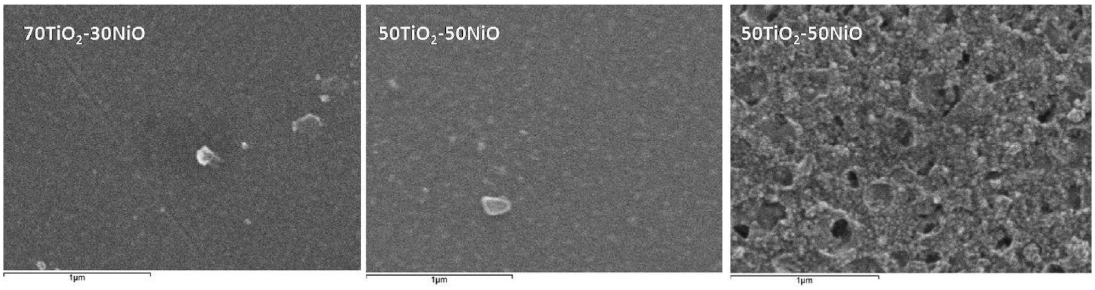

Figure 3. Bright field SEM images of the surface of different films containing Au NPs annealed at 500 °C. The scale bar is 1 μm.

Table 2. Chemical Composition (atomic) of the Au−TiO_2−NiO Nanocomposite Films Annealed at 500 °C Evaluated with SEM-EDX by Positioning the Electron Beam on Five Different Regions of Each Sample[a]

sample	% C	% O	% Si	% Ti	% Ni	Ti:Ni ratio (experimental)	Ti:Ni ratio (nominal)
70TiO_2−30NiO	19.4	54.3	25.2	0.82	0.37	2.2	2.3
50TiO_2−50NiO	18.3	55.3	24.8	0.79	0.73	1.1	1.0
30TiO_2−70NiO	17.9	57.9	23	0.31	0.85	0.4	0.4

[a] Because all the films were deposited on silica glass, only the levels of Ti and Ni refer to film composition, while the levels of oxygen and silicon are due also to the substrate. Au is not reported as it was used as the conductive coating.

sol−gel matrix). All samples annealed at 600 °C show $NiTiO_3$ peaks, while Ti-rich and Ni-rich samples also show TiO_2−rutile and NiO peaks, respectively. It is worth noting that diffraction peaks of the samples containing Au NPs are slightly more intense and sharper if compared to the peaks of the samples without gold, indicating a larger amount of crystalline phase, and larger crystallite size. As shown in Table 1, a clear increase in crystal size is observed in Au−TiO_2−NiO samples for all the crystalline phases.

From scanning electron microscope (SEM) images reported in Figure 3, one can see that an increase in the amount of NiO leads to a more irregular and crystalline film, also confirmed by XRD data. The difference in morphology can be easily related to the different amount of nickel ions in the sol−gel solution: in fact, thin films prepared from titanium alkoxide precursors are usually homogeneous and have a low degree of surface roughness,[57,58] while solutions of nickel salts dissolved in only a solvent usually lead to less homogeneous and rougher films.[59] Energy dispersive X-ray (EDX) results in terms of average atomic percentage are listed in Table 2, together with the experimental and theoretical Ti:Ni ratios: the sample composition is confirmed here, taking into account that the error for the EDX measurement is around 5%.

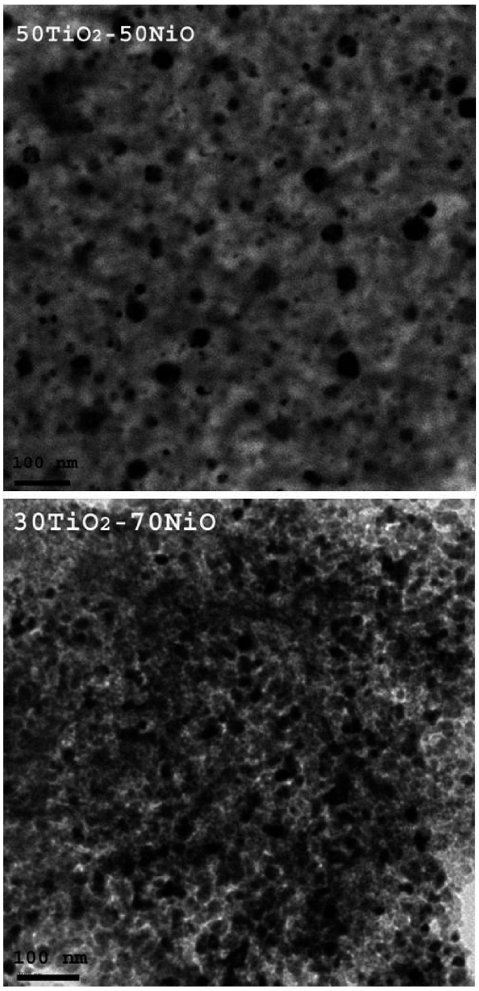

Figure 4. Bright field TEM images of Au−TiO_2−NiO nanocomposite films annealed at 500 °C. Au NPs are clearly detectable as darker spots. The scale bar is 100 nm.

Transmission electron microscopy (TEM) analysis (Figure 4) revealed the presence of polydispersed Au NPs (σ = 4.2 nm) with an average diameter of 13 nm. The visual contrast of the image in bright field TEM is related to two factors: mass−thickness contrast and scattering (diffraction) contrast. Elements with high atomic numbers (in this case, Au) maximize both components, with respect to the lighter oxide matrix components, so Au NPs appear in bright field TEM images as darker spots. Only for the Ni-rich sample can another crystalline phase (NiO) be detected inside the amorphous matrix, as confirmed also by the XRD data. Polydispersion of Au NPs comes from the poor control on the reduction process of Au^{3+} ions inside the film: immediately after the deposition, there is no evidence of metallic gold inside the matrix, because the reduction occurs during the annealing process due to the thermal decomposition of gold chloride species

---

(57) Yu, J.; Yu, J. C.; Cheng, B.; Zhao, X.; Zheng, Z.; Li, A. S. K. *J. Sol-Gel Sci. Technol.* **2002**, *24*, 229.

(58) Medina-Valtierra, J.; Frausto-Reyes, C.; Calixto, S.; Bosch, P.; Hugo Lara, V. *Mater. Charact.* **2007**, *58*, 233.

(59) Sharma, P. K.; Fantini, M. C. A.; Gorenstein, A. *Solid State Ionics* **1998**, *113*−*115*, 457.

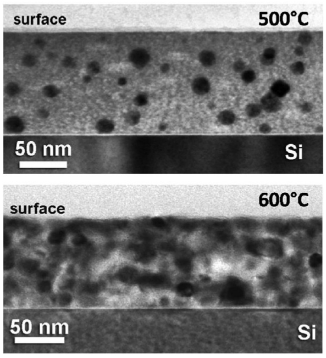

Figure 5. Bright field cross-sectional TEM images of the Au−70TiO_2−30NiO nanocomposite film deposited on the Si substrate and annealed at 500 and 600 °C. Au NPs are clearly visible as darker spots in the 500 °C sample, while after the sample has been annealed at 600 °C, the crystalline phases of the matrix also appear with a higher contrast. The scale bar is 50 nm.

(first a reduction from $AuCl_3$ to AuCl around 160 °C and then a second reduction to metallic gold at ∼200 °C) and oxidation of the organic compounds that can act as reducing agents, donating electrons to gold ions and thereby leading to Au NP nucleation.[60,61]

Cross-sectional TEM images (Figure 5) show Au NPs homogeneously dispersed through the film thickness, but other crystalline phases can be seen in the 600 °C annealed sample. Fast Fourier transform (FFT) analysis of high-resolution TEM images (Figure 6) has been performed to measure lattice distances, and a comparison with theoretical data for different phases has been made. The measured lattice parameters are compatible with Au, TiO_2−rutile, and $NiTiO_3$ phases, although some TiO_2−anatase lattice planes are also present. This can be due to a partial crystallization of anatase that rapidly evolved into the rutile phase, also confirmed by XRD measurements performed on samples treated isothermally at 600 °C for up to 10 h or annealed progressively from 500 to 800 °C (data not shown here). However, comparison with reference TiO_2 and Au−TiO_2 thin films shows crystalline titania only in the anatase phase, even with the 600 °C treatment, while rutile is observed only for a higher annealing temperature, when the anatase crystals grow; therefore, the rutile phase becomes more stable, as described elsewhere.[62] Thus, the presence of nickel inside the matrix triggers the crystallization of TiO_2 in the rutile phase for low temperatures and small crystallite sizes, even if a partial transition process from amorphous to anatase and then to rutile is observed.

From the cross-sectional HR-TEM images reported in Figure 5, the porosity of the film can be also recognized: the sample annealed at 500 °C exhibits higher porosity than the sample treated at 600 °C, but even after being annealed at 600 °C, the film is still porous. In addition, both samples are slightly more dense near the surface. Ellipsometric measurements performed on these samples confirmed the thicknesses measured by TEM and revealed, even after 600 °C annealing, a low refractive index, if compared to the expected value for a dense film with the same chemical and morphological composition, thereby highlighting the residual porosity of the nanocomposite films.

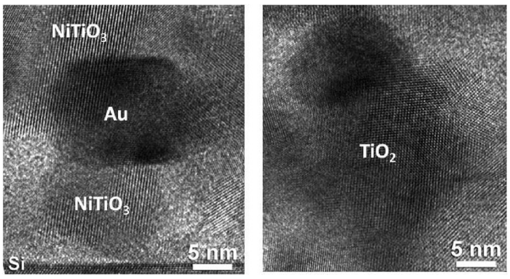

Figure 6. Bright field HR-TEM images of a Au−70TiO_2−30NiO nanocomposite film annealed at 600 °C highlighting the formation of TiO_2, $NiTiO_3$, and Au nanocrystalline phases. The scale bar is 5 nm.

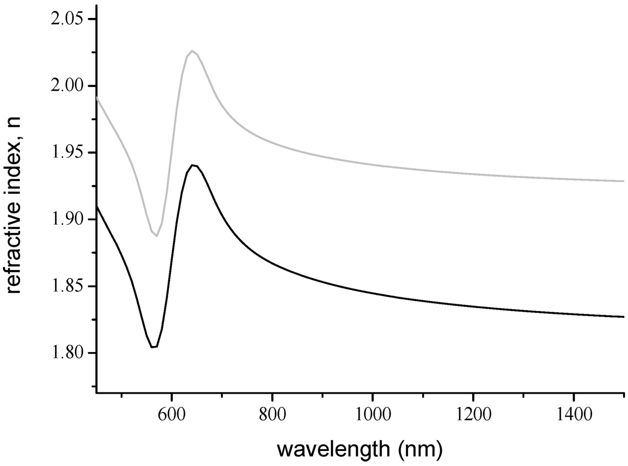

Figure 7. Refractive index dispersion curves of a 50TiO_2−50NiO film with Au NPs annealed at 500 °C, measured at room temperature under nitrogen (black line) and ethanol vapor (light gray line) atmospheres.

Refractive index values of all the samples are always less than 2 in the 800−1500 nm wavelength range, even after 600 °C annealing: considering that the refractive index values for dense and fully crystalline $NiTiO_3$, TiO_2−rutile, and NiO are 2.4, 2.7, and 2.18, respectively,[63−65] there is a large difference between measured and tabulated values, which can be ascribed to both the amorphous nature and porosity. To gain a more accurate indication on the porosity of such samples, ellipsometric analyses were performed under nitrogen and ethanol vapor atmospheres: pores are filled with nitrogen in the first case and with ethanol in the second one. The measured refractive index values can be written as follows:

$$n_{\mathrm{N}} = Xn_{\mathrm{N}}^{\mathrm{matrix}} + (1-X)n_{\mathrm{N}}^{\mathrm{pores}}$$

$$n_{\mathrm{E}} = Xn_{\mathrm{E}}^{\mathrm{matrix}} + (1-X)n_{\mathrm{E}}^{\mathrm{pores}}$$

---

(60) Johnson, B. F. G.; Davis, R. *Comprehensive Inorganic Chemistry*; Bailer, J. C., Jr., Emeleus, H. J., Nyholm, R., Trotman-Dickenzon, A. F.; Pergamon: NewYork, 1973; Vol. *3*, p 129.

(61) Hirai, H.; Nakao, Y.; Toshima, N. *J. Macromol. Sci. Chem.* **1979**, *A13*, 727.

(62) Zhang, H.; Banfield, J. F. *J. Phys. Chem. B* **2000**, *104*, 3481.

(63) Taylor, D. J.; Fleig, P. F.; Page, R. A. *Thin Solid Films* **2002**, *408*, 104.

(64) Lide, D. R. *Handbook of Chemistry and Physics*, 72nd ed.; CRC Press: Boca Raton, FL, 1991; pp 4−108.

(65) Lide, D. R. *Handbook of Chemistry and Physics*, 72nd ed.; CRC Press: Boca Raton, FL, 1991; pp 4−78.

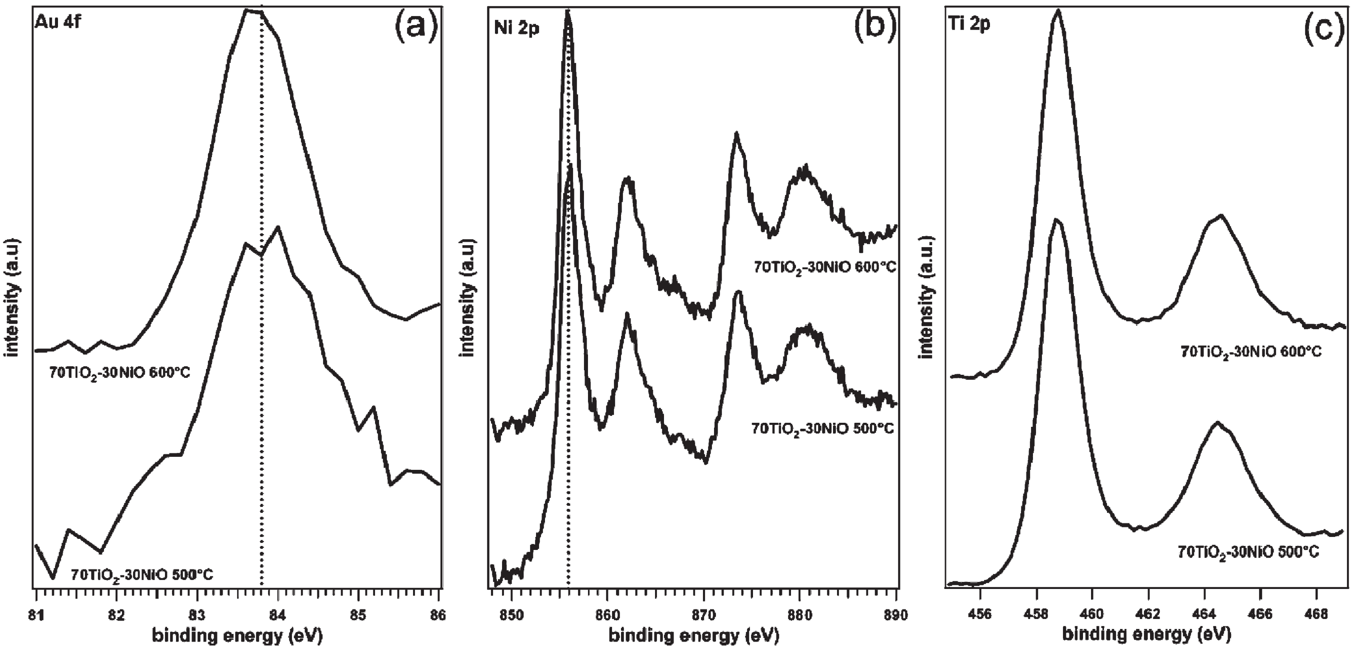

Figure 8. Al Kα excited XPS core level regions for a $70TiO_2-30NiO$ nanocomposite film containing Au NPs annealed at 500 and 600 °C.

where N, E, and X represent nitrogen, ethanol, and the matrix volume fraction, respectively. By subtracting the two equations and realizing that the refractive index of the matrix is obviously the same in both measurements, and that the refractive index values of the pores filled with nitrogen and ethanol are basically the values for pure nitrogen ($n = 1$) and ethanol ($n = 1.36$), respectively, we are able to isolate the pore volume fraction as a function of the measured refractive index:

$$1-X = \frac{n_{\mathrm{E}} - n_{\mathrm{N}}}{n_{\mathrm{E}}^{\mathrm{pores}} - n_{\mathrm{N}}^{\mathrm{pores}}}$$

Figure 7 shows the refractive index dispersion curves measured in nitrogen and ethanol vapors for a $50TiO_2-50NiO$ sample containing Au NPs annealed at 500 °C; at 1100 nm, the difference in the refractive index is 0.098, leading to a porosity volumetric fraction of ~27%. Similar values of porosity fraction have been evaluated for the other samples with different compositions. It is noteworthy that this method underestimates the porosity, because it takes into account only open porosity and it is hard to specifically determine if ethanol enters all the open pores; therefore, this evaluation is on the conservative side, and it is reasonable to assume that the porosity is at least 27%.

To achieve a surface characterization of the studied films, we have measured the core level photoemission data obtained by using the XPS of the whole set of samples. However, differences are irrelevant in the XPS data of the samples with different TiO_2-NiO compositions, and for this reason in Figure 8, we report only the investigated XPS regions (i.e., Ni 2p, Ti 2p, and Au 4f) for the $Au-70TiO_2-30NiO$ nanocomposite sample [i.e., the most significant composition of the films in relation to gas sensing performance (see below)] after annealing at 500 and 600 °C. The Ni 2p spectra are indicative of stoichiometric NiO, as evidenced by the position of the binding energy (BE) of the Ni $2p_{3/2}$ component (855.8 eV), as well as by the intensity and energy spacing of the higher BE satellite lines. In the case of the Ti 2p photoemission spectra, the Ti $2p_{3/2}$ peak is centered at 459 eV and is characterized by a full width at half-maximum (fwhm) compatible with just one component indicating the presence of fully stoichiometric TiO_2. It can also be seen that core level XPS data do not undergo any significant change as a consequence of thermal annealing from 500 to 600 °C: there is no modification either in the energy position or in the fwhm of both Ti and Ni photoemission lines. Even so, the fingerprint of the $NiTiO_3$ species would be quite difficult to resolve between NiO and TiO_2, since the oxidation state of Ni^{2+} and Ti^{4+} is unaltered, so the presence of $NiTiO_3$ cannot be excluded.[66] However, from the surface stoichiometries obtained by XPS after annealing at 500 and 600 °C (see Table 3 and compare with the corresponding data of bulk composition reported in Table 2), a surface segregation of the NiO component with respect to TiO_2 can be clearly observed. In addition, it can be seen that the surface stoichiometries of the samples treated at the two different annealing temperatures (500 and 600 °C) remain essentially the same, excluding therefore any annealing-induced surface segregation phenomenon, albeit in the explored temperature range.

The Au $4f_{7/2}$ photoemission line is centered for all samples at 83.8 eV which is in good agreement with the value reported for bulk metal Au (84.0 eV). The very small shift to a lower BE can be attributed to the presence of very small particles with an extended Au−O interface.

---

(66) Atuchin, V. V.; Kesler, V. G.; Pervukhina, N. V.; Zhang, Z. *J. Electron Spectrosc. Relat. Phenom.* **2006**, *152*, 18.

Table 3. Surface Stoichiometries Derived from XPS Data of the Investigated $70TiO_2-30NiO$ Film with Au NPs

	atomic percent (%)	
	500 °C	600 °C
Ni	12	12
Ti	16	16
O	55	53
Au	0.1	0.3
C	17	18.7

Again, in the case of Au, no BE change can be observed for the sample treated at higher temperatures. The contribution to surface stoichiometry from the Au NPs (Table 3) is below the nominal bulk values (Table 2), indicating that they are predominantly located in the film bulk, in agreement with the cross-sectional HR-TEM images reported in Figure 5. A somewhat higher signal-to-noise ratio observed in the higher-temperature sample is connected to the almost triple value evidenced in Table 3, which is possibly related to some temperature-induced surfacing of Au NPs in the higher-temperature sample, which can be seen in Figure 5.

To explore the possible presence of interfacial states among the TiO_2 and NiO nanocomposite components, we have also measured the valence-band (VB) region of the TiO_2-NiO films with different compositions using UPS. The corresponding data are reported and assessed in the Supporting Information. According to them, we suggest that the films are a simple mechanical blend of the parent oxides and that possible interfacial states due to the previously observed Au−NiO epitaxial growth[56] are hardly visible when such a standard UPS technique is adopted.

Gas Sensing Tests. The nanocomposite films have been subjected to gas sensing tests according to the procedure described in Experimental Procedures. Samples without Au did not give any appreciable response to any of the tested gases, while thin films containing Au NPs gave a good response to only H_2S; therefore, all results reported here refer to the Au-containing samples. Exposure to CO, H_2, or propane produced almost no variation in the absorption spectra. Figure 9a shows the optical absorption spectra of the $Au-50TiO_2-50NiO$ film annealed at 500 °C and collected at the operative temperature (OT) of 350 °C in air and after H_2S exposure. Tests at lower temperatures have also been performed, giving a weak or null response up to 200 °C. Tests at an OT of 300 °C had quite good response but with longer recovery times, and the baseline sometimes was not fully recovered; therefore, each test reported here, if not specified, has been performed at an OT of 350 °C.

A Au surface plasmon resonance (SPR) peak centered around 590 nm is clearly visible in the optical absorption spectrum; the peak wavelength position is substantially smaller than the expected value for Au NPs of the same size in a TiO_2-NiO matrix, considering the tabulated refractive indexes for the two oxides: this is due to the residual porosity of the film, as described before, that lowers the average refractive index, causing a blue shift of the Au SPR peak. This behavior has been observed in all the samples prepared.

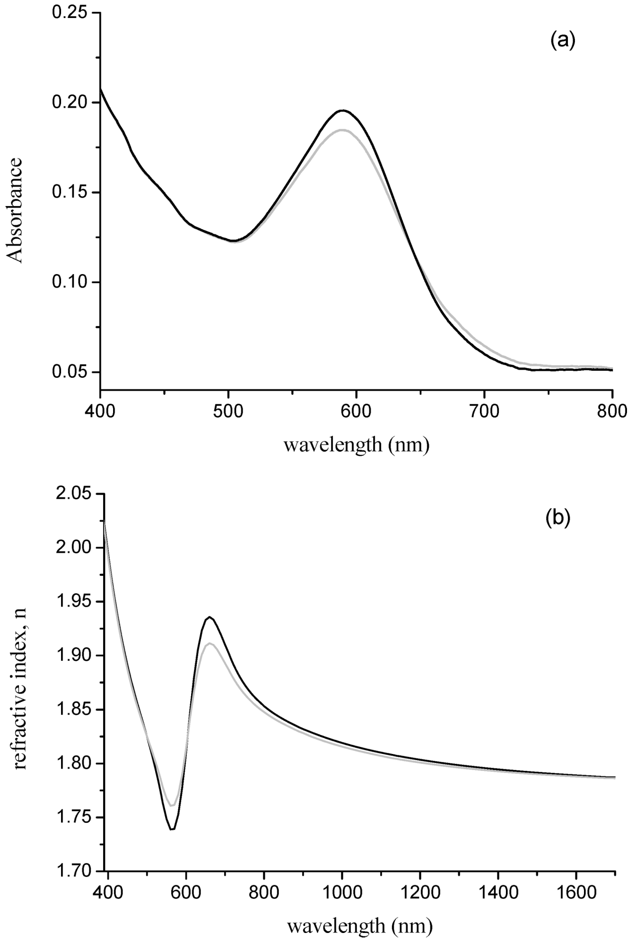

Figure 9. (a) Absorption spectra of a $50TiO_2-50NiO$ film with Au NPs annealed at 500 °C measured in air (black line) and during exposure to 0.01% (v/v) H_2S (light gray line) at an OT of 350 °C. The figure highlights the effect of gas exposure on the surface plasmon resonance frequencies of Au NPs (500−750 nm region). (b) Refractive index dispersion curves of a $70TiO_2-30NiO$ film with Au NPs annealed at 500 °C before H_2S exposure (black line) and after the "freezing" process (light gray line).

During H_2S exposure, the form of the Au plasmon peak undergoes distinctive changes, i.e., a decrease in maximum intensity and a broadening especially at high wavelengths, while no shifts in the frequency of the peak have been observed in all the Au-containing samples (see Figure 2 of the Supporting Information). This behavior suggests an interaction between H_2S and the surface of Au NPs, which leads to a reduction in the number of surface oscillating free electrons, due to a charge transfer between Au and S, with a depletion of Au d-electrons, that provides a decay path for excited s-electrons, spreading the surface plasma resonance over a wider range of wavelengths, damping and broadening the plasmon peak. The same behavior has also been observed on thin films composed of Au NPs dispersed inside a SiO_2 matrix, where no interaction is established between the target gas and the inert oxide matrix, so the variation in the optical properties is due to the interaction of hydrogen sulfide with Au particles.

Ellipsometric analyses performed on samples exposed to H_2S at high temperatures and cooled at room temperature under H_2S [sample named "frozen" (see the

Supporting Information for details)] revealed a difference in the dielectric properties compared to those of pristine unexposed films only in the Au SPR wavelength range, while almost no variations in the refractive index are observed in the nonabsorbing region (Figure 9b). Au-free samples did not present any relevant change in either refractive index or absorption coefficient, suggesting again a key role played by Au NPs in the interaction with the target gas.

Significant sensitivity changes are observed in the films with different compositions, as seen in Figure 10a: the absorbance variation is lower for the NiO-rich nanocomposite film, while $50TiO_2-50NiO$ and $70TiO_2-30NiO$ films exhibited very similar behavior. Interestingly, the $70TiO_2-30NiO$ nanocomposite film shows the best dynamic behavior, with a fast response after initial hydrogen sulfide exposure, a stable signal during the gas flow phase, and good recovery of the baseline level, as seen in Figure 10b. We observed that the dynamic variation of absorption measured at the maximum sensitivity wavelength [maximum of the optical absorption change (OAC) of Figure 10a] is greater in $50TiO_2-50NiO$ and $70TiO_2-30NiO$ samples than in the $30TiO_2-70NiO$ sample, but the Ti-rich sample shows also a slightly more stable signal and a faster recovery compared to the $50TiO_2-50NiO$ film. As expected, all samples show almost no variation during hydrogen exposure, while the $Au-TiO_2$ reference sample gives a response to H_2S but also to both CO and H_2, as already known from our previous work.[67]

Because of the strong SPR of Au NPs in the visible region, the optical response of the sensor can be tuned by choosing an appropriate wavelength of analysis, as reported in literature for some oxide thin films containing Au NPs.[68] From the form of the OAC curves in Figure 10a, a negative minimum and a positive maximum can be determined. Exposure to H_2S leads to a decrease in the optical absorption of the sample if the testing wavelength is near the minimum of the OAC curve, as reported in Figure 10b, while operating near the maximum of the OAC curve will lead to an increase in optical absorption. It is also possible to recognize some wavelengths in which the sensor response is null: this behavior allows the operator to tune the sensitivity of the optical sensor by selecting the analysis wavelength. Moreover, different gases usually promote different optical variations, so in principle, it is possible to selectively detect one particular gas inside a complex gas mixture by using wavelength modulation.[69,70]

As one can see from Figure 11a, the optical sensitivity of the nanocomposites annealed at 600 °C is higher with respect to those annealed at 500 °C. Also, the dynamic behavior (Figure 11b) is improved by the thermal treatment, and the response time is very fast (~20 s to reach 90% of the total variation). There is a stable signal during hydrogen sulfide exposure, and the recovery of the baseline is almost perfect and rapid. This improvement of sensor performance can be directly related to the microstructure of the nanocomposite film: the annealing process induces further crystallization without compromising the porosity of the matrix, as confirmed by TEM and the ellipsometry measurements previously reported.

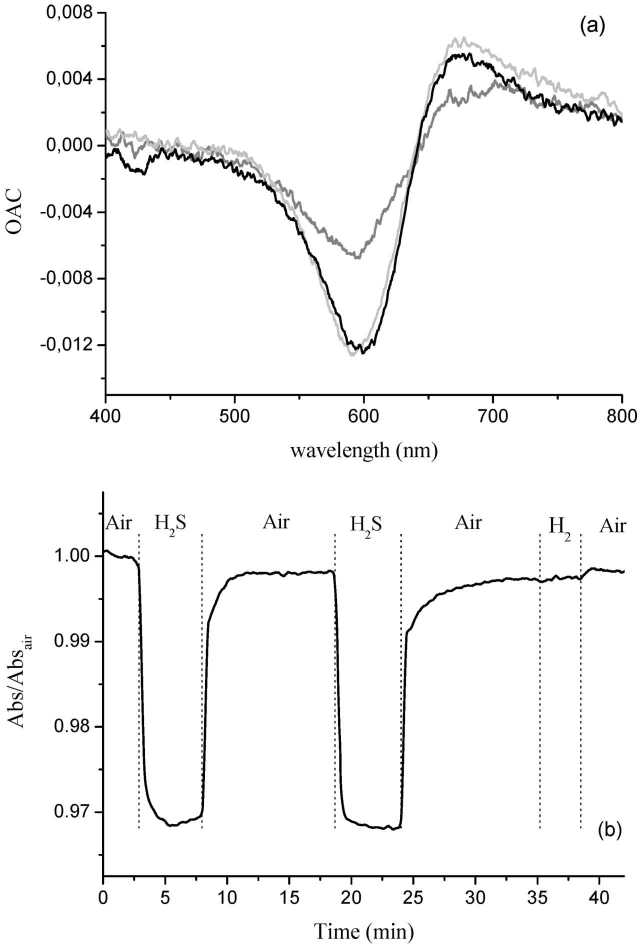

Figure 10. (a) Optical absorbance change (OAC = $A_{gas} - A_{air}$) of $70TiO_2-30NiO$ (black line), $50TiO_2-50NiO$ (light gray line), and $30TiO_2-70NiO$ (gray line) films containing Au NPs annealed at 500 °C after exposure to 0.01% (v/v) H_2S at an OT of 350 °C. (b) Dynamic response of $Au-70TiO_2-30NiO$ nanocomposite films annealed at 500 and 350 °C and at 605 nm under exposure to to air−0.01% H_2S−air−0.01% H_2S−air−1% H_2−air cycle.

To check cross sensitivity to another gas species, during H_2S (0.01%) exposure, H_2 (1%) was introduced inside the test cell, keeping the total flow rate constant. As one can see from Figure 11b, there is almost no response to hydrogen: this result confirms that the $Au-70TiO_2-30NiO$ sample can selectively detect hydrogen sulfide in a 100:1 H_2/H_2S mixture in air.

Further experiments with samples treated at 600 °C were performed with lower H_2S concentrations, and the results are reported in Figure 12: upon examination of the spectrum in Figure 12a, the absorption value during 10 and 100 ppm H_2S exposure is almost the same, but the dynamic performance is slightly different. This behavior suggests a saturation of reactive sites of the sample, even

---

(67) Buso, D.; Post, M.; Cantalini, C.; Mulvaney, P.; Martucci, A. *Adv. Funct. Mater.* **2008**, *18*, 3843.
(68) Ando, M.; Kobayashi, T.; Iijima, S.; Haruta, M. *Sens. Actuators, B* **2003**, *96*, 589.
(69) Ando, M.; Kobayashi, T.; Haruta, M. *Catal. Today* **1997**, *36*, 135.
(70) Buso, D.; Busato, G.; Guglielmi, M.; Martucci, A.; Bello, V.; Mattei, G.; Mazzoldi, P.; Post, M. L. *Nanotechnology* **2007**, *18*, 475505.

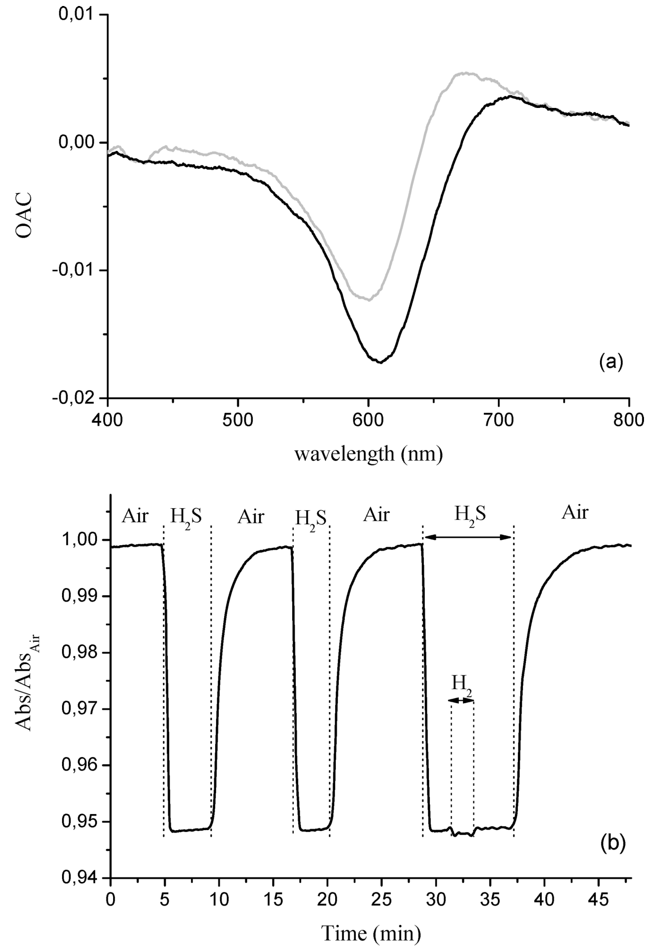

Figure 11. (a) Optical absorbance change (OAC = $A_{gas} - A_{air}$) of a Au−70TiO$_2$−30NiO nanocomposite film annealed at 500 °C (gray line) and 600 °C (black line) after being exposed to 0.01% (v/v) H_2S at an operative temperature (OT) of 350 °C. (b) Dynamic response at 605 nm of a Au−70TiO$_2$−30NiO film annealed at 600 °C under exposure to an air−0.01% H_2S−air−0.01% H_2S−air−0.01% H_2S/1% H_2−air cycle at an OT of 350 °C.

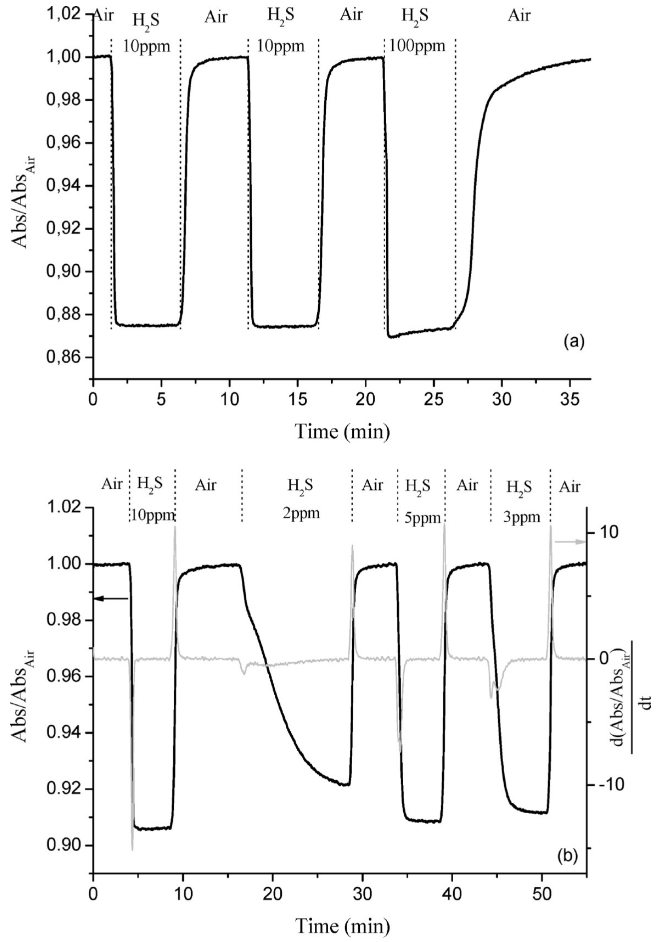

Figure 12. (a) Dynamic response at 605 nm of a Au−70TiO$_2$−30NiO nanocomposite film annealed at 600 °C after exposure to an air−0.001% H_2S−air−0.001% H_2S−air−0.01% H_2S−air cycle at an OT of 350 °C. (b) Dynamic response at 590 nm of a Au−50TiO$_2$−50NiO nanocomposite film annealed at 600 °C after exposure to an air−10 ppm H_2S−air−2 ppm H_2S−air−3 ppm H_2S−air−5 ppm H_2S−air−3 ppm H_2S−air cycle at an OT of 350 °C (black line) and the derivative of this spectrum (gray line).

with 10 ppm, so an equilibrium between the absorption and desorption of H_2S over the active surface occurs. Moreover, from the gas-to-air transient, a slower recovery of the baseline is observed after 100 ppm exposure, indicating a slower desorption of hydrogen sulfide and reaction products from the reactive sites. This can be related to the longer time needed to complete the evacuation of the test chamber after 100 ppm H_2S exposure, compared to 10 ppm exposure, the flow rate being constant during the different tests.

Figure 12b reports a dynamic test with H_2S concentrations ranging from 2 to 10 ppm and the derivative of this spectrum: the saturation is still reached with 5 ppm H_2S, while the absorption change during 3 and 2 ppm exposure is slightly lower, indicating that around 4 ppm H_2S is the threshold for saturation of reactive sites. In addition, a decrease in target gas concentration produces longer response times, while for quite low concentrations, i.e., up to 10 ppm, recovery times are not affected by hydrogen sulfide concentration. This effect can be clearly seen in the derivative spectrum, where the negative peaks represent the air-to-gas transient and the positive peaks represent the gas-to-air transient. Comparing these peaks, we can see that the desorption behavior is very similar for the different concentrations (positive peaks are comparable in intensity and broadening) whereas absorption behavior changes significantly. Higher concentrations lead to very sharp and intense peaks (very fast response), while low concentrations result in broad and less intense peaks, indicating longer response times.

The material is therefore sensitive also to very low concentrations of H_2S, with response and recovery times strongly related to gas concentration: for high concentrations (100 ppm), the recovery behavior is worse than at lower concentrations, indicating a desorption equilibrium, while for very low concentrations (few parts per million), the response time increases and eventually results in a saturation of reaction sites for H_2S concentrations of > 3 ppm.

Finally, we want to briefly discuss the possible mechanisms for interaction between H_2S and the sensor. It is well-known that one of the most common ways to remove hydrogen sulfide from waste gases generated in industrial processes and to produce sulfur is the Claus method, a two-step reaction in which hydrogen sulfide is first thermally oxidized to sulfur dioxide (SO_2) and water at a high temperature (usually around 1000 °C) and then a catalytic reaction between SO_2 and H_2S takes place at a lower temperature (around 300 °C), over some particular catalysts, leading to the formation of water and elemental sulfur.[71-73] The main reason for the development of this two-step process is that the direct oxidation of H_2S to elemental sulfur, although thermodynamically favored at low temperatures, has a very low rate and yield of conversion, while the complete oxidation of H_2S to SO_2 can be achieved only at high temperatures, for thermodynamic reasons.[74]

It has also been reported that exposing metal oxides (like CuO, SnO_2, WO_3, and Cr_2O_3) to H_2S at quite low temperatures (<400 °C) usually leads to the formation of metal sulfides, which can then be oxidized by treatment in oxygen or air, resulting in the formation of the initial oxide and of gaseous SO_2.[75-77] The sensing properties of these kinds of materials are related to the different electric conductivity of sulfide species compared to that of the initial oxide: a variation in resistivity is thus generated, which can be easily detected and related to H_2S content. However, it has been demonstrated by a focused surface science study[78] that H_2S absorbed on TiO_2 reacts at temperatures above 300 °C with surface oxygen and forms SO_2 which easily desorbs from TiO_2. It is noteworthy that a similar temperature range is required for the gas sensing activity of the presently studied nanocomposites. As a result, according to this whole body of data, it is reasonable to propose that SO_2 is the product of the interaction of H_2S with the present nanocomposite sensor.

To demonstrate the presence of SO_2 in the exhaust gases of the sensor films under working conditions, Radiello diffusion samplers were used as described in Experimental Procedures. For this particular experiment, a $70TiO_2-30NiO$ film containing Au NPs annealed at 500 °C was used, and the operating temperature was 350 °C. Sulfur dioxide was clearly detected as a reaction product, in an amount which increased with exposure time, confirming that the reaction of H_2S with the sensor consumes the target gas.

The formation of SO_2 can be related to two different processes: either catalytic oxidation of H_2S over the $Au-TiO_2-NiO$ nanocomposite or the rapid formation and decomposition of sulfide species due to reactions of the oxide matrix with H_2S and O_2.

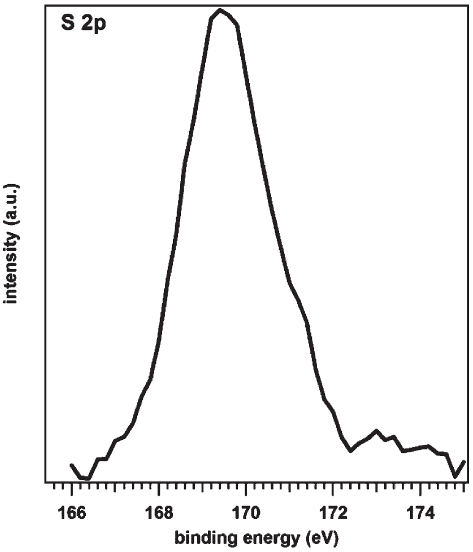

Figure 13. XPS S 2p region of the Au-doped $70TiO_2-30NiO$ film annealed at 500 °C after the exposure to H_2S.

Some evidence of the actual mechanism operating in our sensors comes from XPS analysis performed on the $70TiO_2-30NiO$ frozen sample, containing Au NPs and annealed at 500 °C. In these data, the S 2p photoemission peak (see Figure 13) is centered at 169.5 eV, indicating the presence of highly oxidized SO_x species, i.e., SO_2,[79] while no evidence of sulfides has been found. In addition, no changes can be seen before or after the H_2S dosing from the analysis of the XPS spectra of Au 4f, Ti 2p, and Ni 2p, and no modifications in XRD diffraction peaks can be envisaged either. This evidence supports a direct catalytic oxidation of H_2S rather than a metal sulfide-mediated transformation. However, with regard to the role of Au in such a process, there is no direct evidence of that, except indirectly from the ellipsometric analyses performed on the frozen samples which suggests that the optical response is due to an interaction of the gas with the Au NPs. Most probably, XPS does not provide sufficient sensitivity to directly monitor the interaction of H_2S with the few and mostly embedded Au NPs. Therefore, the evidence so far suggests that the probable mechanism for the overall process is a first interaction of H_2S with the surface of Au NPs, which can be easily monitored from the modification of the Au SPR peak shape, and then a second step involving the catalytic oxidation of H_2S to SO_x occurs, as confirmed by Radiello sampler analysis combined to XPS and XRD measurements that show no formation of metal sulfides.

As known from Mie theory (and its extensions) and also reported in the literature,[80,81] a shell of a material with a high refractive index on Au NPs will produce a red shift of the Au SPR band, also with a very thin shell, while in our sample, no shift can be seen after H_2S interaction.

---

(71) Piéplu, A.; Saur, O.; Lavalley, J. C.; Legendre, O.; Nédez, C. *Catal. Rev.* **1998**, *40*(4), 409.

(72) Gamson, B. W.; Elkins, R. H. *Chem. Eng. Prog.* **1953**, *49*, 203.

(73) Ferguson, P. A. *Hydrogen Sulfide Removal from Gases Air, and Liquids*; Noyes Data Corp.: Park Ridge, NJ, 1975.

(74) Baglio, J. A.; Susa, T. J.; Wortham, D. W.; Trickett, E. A.; Lewis, T. J. *Ind. Eng. Chem. Prod. Res. Dev.* **1982**, *21*, 408.

(75) Reyes, L. F.; Hoel, A.; Saukko, S.; Heszler, P.; Lantto, V.; Granqvist, C. G. *Sens. Actuators, B* **2006**, *117*, 128.

(76) Brauer, G. *Handbook of Preparative Inorganic Chemistry*; Academic Press: NewYork, 1965; Vol. , *2*.

(77) Pagnier, T.; Boulova, M.; Galerie, A.; Gaskov, A.; Lucazeau, G. *Sens. Actuators, B* **2000**, *71*, 134.

(78) Yanxina, C.; Yia, J.; Wenzhaoa, L.; Rongchaoa, J.; Shaozhenb, T.; Wenbin, H. *Catal. Today* **1999**, *50*, 39.

(79) Sayago, D. I.; Serrano, P.; Boehme, O.; Goldoni, A.; Paolucci, G.; Román, E.; Martín-Gago, J. A. *Phys. Rev. B* **2001**, *64*, 205402.

(80) Tom, R. T.; Sreekumaran Nair, A.; Singh, N.; Aslam, M.; Nagendra, C. L.; Philip, R.; Vijayamohanan, K.; Pradeep, T. *Langmuir* **2003**, *19*, 3439.

(81) Oldfield, G.; Ung, T.; Mulvaney, P. *Adv. Mater.* **2000**, *12*, 1519.

A set of simulations has been performed considering a core shell structure in which an Au core with a radius of 10 nm is surrounded by a shell with an increasing thickness of Au_2S (see the Supporting Information for details). A shift of 2 nm in the SPR position is already detectable with a shell of 0.2 nm. Since no such shift has been measured in our samples, we exclude the formation of a shell of sulfide, because in that case we should experience a shift of the SPR peak. Moreover, in all three different samples (that have Au SPR at different wavelengths, coming from different refractive indexes of the matrix), there is no shift of the SPR band upon exposure to H_2S (Figure 2 of the Supporting Information), so even in the very particular case in which the Au sulfide shell matches exactly the refractive index of the surrounding matrix, this could happen only in one of the three cases; therefore, we can assume that no change in the refractive index around the gold NPs is happening.

Besides, it has been demonstrated[82] that the Au−S bond decomposes in air in the 490−525 K range (217−252 °C): since our experiments have been conducted at 350 °C, no Au sulfide species can exist at that temperature.

What we suggest is an interaction between sulfur atoms and the surface of Au NPs, the nature of this bond being intermediate between a covalent bond and a coordination bond[83] leading to a surface passivation of the metal, depleting Au d-electrons and so reducing the intensity of the Au SPR peak.

Conclusions

TiO_2−NiO thin films containing Au NPs were synthesized by the sol−gel technique. Structural and morphological characterizations after 500 and 600 °C thermal annealing demonstrate the crystallization of different phases and also a difference in the electronic structure according to the chemical composition and to the annealing temperature of the prepared samples. Their functionality as optical gas sensors has been analyzed after exposure to H_2, CO, H_2S, and propane, confirming a highly selective response to hydrogen sulfide; the response is wavelength-dependent, allowing the tailoring of sensor selectivity toward interfering gases. The samples are sensitive also at a very low concentration of H_2S (few parts per million), and a correlation between target gas concentration and the sensor dynamic behavior has been presented. A saturation of the response to H_2S is found in the ∼5−10 ppm concentration range.

By analyzing the reaction products and the surface chemistry of the samples after their exposure to H_2S, we demonstrated that SO_2 is generated, and since no evidence of metal sulfide species formation has been found, a direct catalytic oxidation of H_2S over the Au−TiO_2−NiO nanocomposite film can be suggested.

Acknowledgment. This work has been supported through the Progetto Strategico PLATFORMS (PLAsmonic nano-Textured materials and architectures FOR enhanced Molecular Sensing) of Padova University. This paper is issued as National Research Council of Canada, NRCC# 51856. A.M. thanks Fondazione Maugeri for providing Radiello samplers and the related chemical analyses. E.D.G. thanks Fondazione CARIPARO for financial support.

Supporting Information Available: Detailed description of all the characterization techniques and hazardous gas handling, UPS data and discussion, absorption spectra for all Au-doped samples during air and during 100 ppm H_2S flow, simulation of the Au SPR wavelength shift when a shell of Au_2S with an increasing thickness is added around spherical Au NPs with a radius of 10 nm. This material is available free of charge via the Internet at http://pubs.acs.org.

---

(82) Ishikawa, K.; Isonaga, T.; Wakita, S.; Suzuki, Y. *Solid State Ionics* **1995**, *79*, 60.

(83) Sellers, H.; Ulman, A.; Shnidman, Y.; Eilers, J. E. *J. Am. Chem. Soc.* **1993**, *115*, 9389–9401.